applied optics

Comparing the performance of a femto fiber-based laser and a Ti:sapphire used for multiphoton microscopy applications

Juan M. Bueno,* Francisco J. Ávila, and Pablo Artal

Laboratorio de Óptica, Instituto Universitario de Investigación en Óptica y Nanofísica Universidad de Murcia, Campus de Espinardo (Ed. 34), 30100, Murcia, Spain
**Corresponding author: bueno@um.es*

Received 4 March 2019; revised 8 April 2019; accepted 16 April 2019; posted 16 April 2019 (Doc. ID 361635); published 8 May 2019

Ti:sapphire laser systems are the more extended excitation sources in multiphoton (MP) microscopy. Although tunable, the cost, size, and lack of portability often limit their use in some research fields. Femtosecond fiber-based lasers represent an attractive alternative since they are portable, compact, and affordable. Most MP applications using these devices employ wavelengths beyond 1000 nm. This work evaluates the performance of a mode-locked fiber-based laser emitting at 780 nm (within the spectral region often used with Ti:sapphire devices) for use in MP imaging microscopy. MP images acquired with this laser system have been compared with those obtained with a "regular" solid-state source. Results herein show that the images recorded with both laser sources were similar, independently of the depth location of the imaged plane. The structural information contained in the images hardly differed. Moreover, the images of deeper layers improved by means of adaptive optics were also similar. These ultrafast laser sources are expected to enhance the impact of MP microscopy in basic research, as well as in biomedical environments. © 2019 Optical Society of America

https://doi.org/10.1364/AO.58.003830

1. INTRODUCTION

Since the development of nonlinear or multiphoton (MP) microscopy in 1990, this imaging technique has been established as a powerful tool for life-sciences research [1]. It provides submicrometer-resolution images of biological specimens without the need of external dyes. Its inherent confocality allows three-dimensional tissue visualization without having to physically slice the sample [2]. MP imaging modalities, such as two-photon excitation fluorescence (TPEF) and second-harmonic generation (SHG), have the ability to image structures and features at deeper locations, which has opened up new possibilities for basic research and clinical diagnosis [2–4].

Previously predicted by Göppert–Mayer in 1931 [5], MP processes are based on the quasi-simultaneous absorption of two near-infrared photons and the emission of a visible photon. Unlike SHG, in which the emitted photon has exactly half the wavelength (and twice the energy) of each incident individual one, in TPEF part of the incoming energy is lost and the visible photon has a wavelength longer than half of the incident one [2,4].

However, the probability of MP absorption in a medium is extremely low and it can only take place when a very high photon flux is present [6]. This is only possible if a mode-locked (pulsed or high-repetition rate) laser is used. For more than two decades, solid-state laser systems (mainly Ti:sapphire) have extensively been used in MP imaging microscopy. These devices are able to generate pulses with durations between picoseconds and hundreds of femtoseconds (fs), repetition rates of tens of megahertz, and a power up to 1 W. The focusing of this laser beam with an appropriate microscope objective concentrates photons, both temporally and spatially, to greatly increase the effectiveness of MP absorption. Although they offer broad and tunable spectrum in the near-infrared region (700–1000 nm), light of ~800 nm has often been reported as the optimal excitation wavelength for biological tissues [7].

The main disadvantages of this type of laser have been their size and cost. Although both have been reduced in the last years, the latter does not fit yet the budget of many researchers interested in MP applications. Although the stability of the original systems has greatly improved, active cooling is required, and they are considered to be complex by users not familiarized with ultrafast optics. Thus, there is a need for exploring alternative techniques in MP microscopy based on compact and turnkey fs lasers at an affordable price.

One of the options fitting those requirements is a fs fiber laser. This type of laser has been reported to provide high pulse energy, entirely passive mode-locking, and excellent pump absorption [8]. Moreover, active cooling is not needed. The use of these lasers in MP experiments is not new. To the best of our

knowledge, Millar *et al.* previously reported third-harmonic generation imaging microscopy (in a plant leaf) by means of a compact and commercially available fs fiber laser emitting at 1560 nm (50-MHz repetition rate, ~100 fs pulse duration) [9]. A similar device was also used for two-photon fluorescence correlation spectroscopy [10]. Tan and co-workers demonstrated MP imaging using a compact fs fiber laser at 1030-nm wavelength (pulse duration 150 fs, repetition rate 40 MHz) [11]. MP images corresponded to rat tail tendon (SHG signal) and human skin (both SHG and TPEF signals) samples were shown. Liu and co-authors demonstrated a fiber-based probe combined with a fiber laser source (central wavelength of 1060 nm, pulse width of 125 fs, pulse repetition rate of 76 MHz) [12]. They reported MP images from a variety of biological tissues. These pulses were later shortened to ~21 fs and this improved fs fiber laser (1030-nm wavelength, 62-MHz repetition rate) was ideally suited for multimodal biomedical imaging [13].

Perillo *et al.* built a mode-locked ytterbium fiber laser for MP imaging of living deep-tissue brain [14]. That source had a central wavelength of 1060 nm, a repetition rate of 40 MHz, and a compressed pulse width of 81 fs. More recently, another compact home-made high-power fs fiber laser centered at 1010 nm (~300 fs pulses, 80-MHz repetition rate) was reported. TPEF (mouse kidney and brain tissue) and SHG (potato and mouse tail) images were successfully acquired [15].

However, most of these fs fiber lasers provide wavelengths beyond 1000 nm, where the gold-standard solid-state Ti:sapphire laser exhibits poor power efficiency [16]. To our knowledge the performance of fs fiber lasers emitting in the range around 800 nm in MP imaging is lacking in the literature. In this work, we further explore the potential of a compact and cost-effective mode-locked fiber laser for MP imaging microscopy. The technical specifications of this illumination source were chosen to be similar to those of a traditional Ti:sapphire device. A research MP microscope was modified to include a dual illumination pathway combining both laser systems. The imaging performance of these illumination sources was evaluated, compared, and discussed.

2. EXPERIMENTAL SETUP

The custom-built MP microscope previously described in [17] was modified for the purpose of this work (see a simplified schematic in Fig. 1). This consisted of a "regular" Ti:sapphire laser (Mira 900, Coherent; laser #1) and a compact ($20 \times 38 \times 11$ cm^3) and fiber-based laser (FemtoFiber ultra NIR laser, TOPTICA Photonics; laser #2). Repetition rates were 76 and 80 MHz, respectively. Within laser #2, the oscillator generates pulses at a fundamental wavelength of 1560 nm. These are frequency doubled by means of an erbium-doped fiber amplifier to 780 nm. This output is very stable and works reliable just after a push-button start. The actual pulse durations were 217 (#1) and 229 (#2) fs, as measured *in situ* with an autocorrelator. The wavelength was the same for both lasers (780 nm) and both beams were linearly polarized.

A flip mirror (FM1) allowed selecting the desired laser beam. For every analyzed sample, the intensity at the sample's plane was set to be the same for both laser sources (controlled with a variable neutral density filter). The size of the two beams was also ensured to be the same by using a beam expander and an iris aperture. Each beam passes a pair of nonresonant galvanometric mirrors for eventual XY raster scanning and is then focused onto the sample by means of a nonimmersion long working-distance microscope objective (20×, NA = 0.5). A DC motor controlled the depth location of the imaged plane within the sample. The nonlinear signal from the specimen under study travels in the backscattered direction through the same objective and reaches the photo-multiplier tube (PMT) used as detection unit. Spectral filters placed in front of the PMT isolate the MP signals, TPEF (long-pass), and SHG (narrow-band).

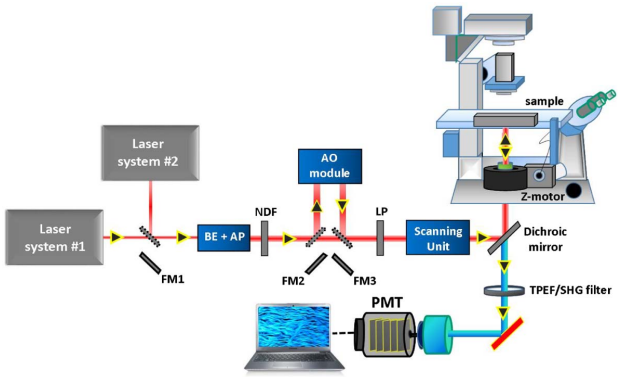

Fig. 1. Schematic diagram of the MP microscope. FM1-FM3, flip mirrors; BE+AP, beam expander and aperture; NDF, variable neutral density filter; LP, linear polarizer; AO module, adaptive optics module; PMT, photo-multiplier tube.

The specimens involved in the experiment provide TPEF and SHG signals. They include corneal, retinal, and skin tissues, and a piece of cellulose. The acquisition time was set to one image per second. Each final image was the average of three individual frames.

To compare the MP images acquired with both laser systems an analysis of the intensity of the images (both TPEF and SHG) was carried out. In addition, sometimes it is also interesting to know if images recorded with different procedures or experimental conditions (laser sources in the present case) provide similar structural information. This is of special interest in images presenting fibrillar structure (for example, collagen-based tissues). For that aim, the structure tensor has been used here [18]. Briefly, this is a useful tool to objectively quantify the organization of a spatially resolved structure. This mathematical procedure is based on the pixel-by-pixel calculation of the partial derivatives of the image along the Cartesian directions. From them, the preferential orientations are computed. The standard deviation of these orientations across the imaged area is defined as the structural dispersion (SD) of the spatial features. In general, the higher the SD, the lower the organization of the sample. Further details on this can be found in [18].

An auxiliary Hartmann–Shack wavefront sensor (not shown in Fig. 1) was used to measure the aberrations of laser beams #1 and #2. The wavefronts were similar: 0.02 and 0.03 μm of root mean square values. More information on the use of this sensor

with high-power laser beams can be found in [19,20]. In addition, a pair of flip mirrors (FM2 and FM3) allows the use of an adaptive optics (AO) module that employs a liquid-crystal-on-silicon spatial light modulator as corrector element. When this AO module is in use, specimen-induced aberrations can be corrected and MP images improved. The AO correction procedure of this module was extensively described elsewhere [17,21]. Here, the AO device will be used to compare the improved MP images provided by both laser systems.

3. RESULTS

A. TPEF and SHG Imaging

Figure 2 presents TPEF images corresponding to a rat retina and a human skin sample acquired with the two lasers. The imaged planes were randomly chosen. Left and central panels share the same color scale for direct comparisons. A visualization of the images reveals that pairs of images look similar. For a better analysis, panels on the right [Figs. 2(e) and 2(f)] show the images resulting from the difference between each pair of images. The mean values of intensity (I_{mean}) indicate the similarity among the images.

To check if the performance of both laser systems is also similar when imaging samples providing SHG signal, the experiment was repeated in corneal tissues under different experimental conditions. Figures 3(a) and 3(b) depict SHG images of an *ex vivo* porcine cornea. The histological section of a human cornea fixed in paraffin is presented in Figs. 3(c) and 3(d). It can be seen that for each pair of SHG images the same features are readily observable. The similarity between the images can be also corroborated by comparing the intensity profiles in a region of interest, as shown in Fig. 3(e). These profiles correspond to the vertical lines in Figs. 3(c) and 3(d).

In addition, Fig. 4 compares the values of total intensity of the MP images in Figs. 2 and 3 acquired with laser systems #1 and #2. A statistically significant linear relationship was found ($R^2 = 0.99$, $p < 0.0001$).

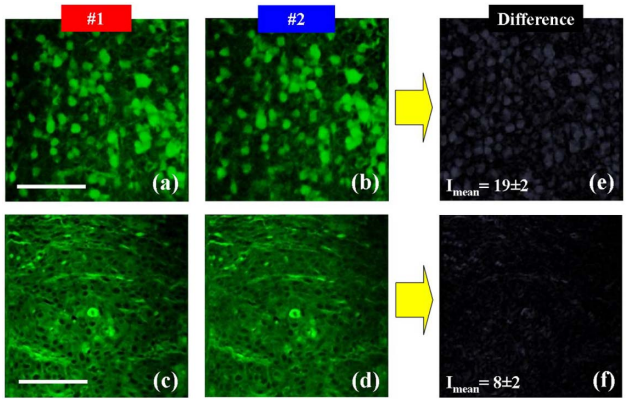

Fig. 2. TPEF images of (a), (b) the ganglion cell layer of rat retina and (c), (d) the human skin epithelium cells acquired with lasers #1 (left panels) and #2 (central panels). Pairs of images are represented with the same color scale. (e), (f) Maps of differences between the corresponding pairs of images. The numbers represent the mean intensity values across the entire image. The average power at the sample's plane was 74 and 37 mW, respectively. Scale bar: 100 μm.

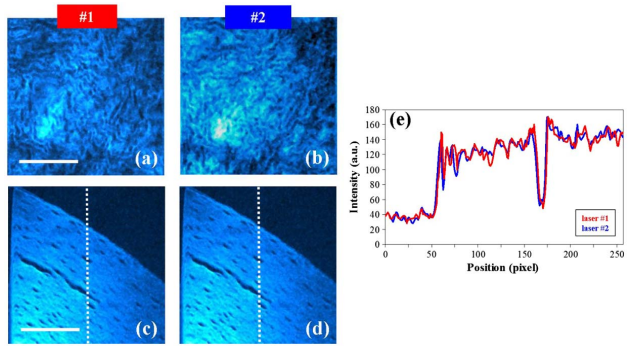

Fig. 3. (a)–(d) SHG images of an *ex vivo* porcine cornea (30-μm depth, 110 mW, upper panels) and a fixed human cornea (10-μm depth, 30 mW, bottom panels) recorded with both laser systems as indicated. Pairs of images share the same color scale. The imaged planes were randomly chosen. Scale bar: 100 μm. (e) Comparison of intensity profiles along the vertical lines traced on (c) and (d).

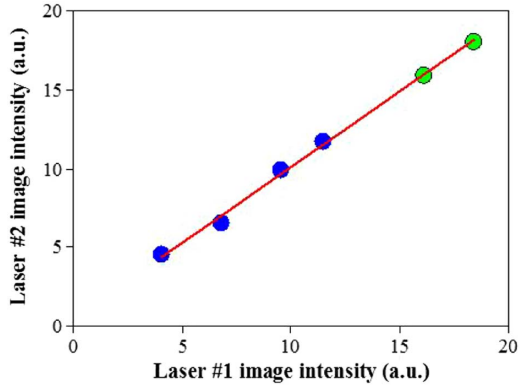

Fig. 4. Relationship between the total intensity of the MP images acquired with both lasers systems and shown in Figs. 2 and 3. Green and blue symbols are associated with TPEF and SHG images, respectively. Red line represents the best linear fit.

The depth location of the previous images was randomly chosen. The comparison of the performance of the two laser systems for different depth locations within the sample is depicted in Fig. 5. A simple visualization reveals once again that the MP images acquired with both laser systems reveal the same features. In particular, this sample shows the two preferential orientations of the fibers arranged in an orthogonal interweaving, typical from bird corneas [22].

For the sense of completeness, apart from the quantitative information provided by the MP intensity levels, it is interesting to show if pairs of images recorded with both laser systems provide the same structural information. As stated above, this has been computed by means of the structure tensor. This will help to test if the information on the images provided by the laser systems #1 and #2 differs. In particular, the histograms of preferential orientation of the collagen fibers in SHG images of Fig. 5 are presented in Fig. 6.

As expected, the parameters of the structure tensor give additional information on the spatial distribution of the imaged

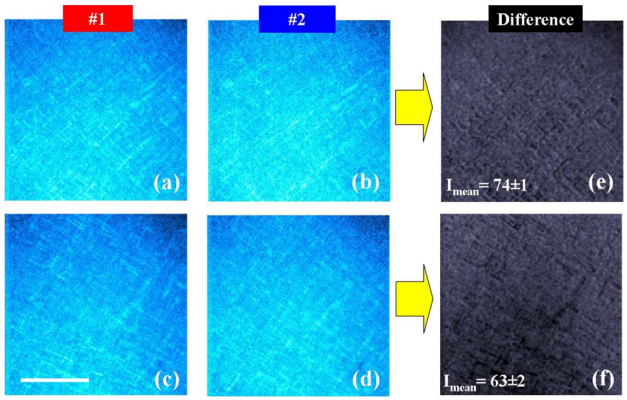

Fig. 5. SHG images of an *ex vivo* eagle cornea at two different depth locations acquired with (a), (c) laser systems #1 and (b), (d) #2. Depth locations are 20 (upper panels) and 50 µm (bottom panels). Maps on the right (e), (f) represent the differences between pairs of images. The average power at the specimen plane was 148 mW. Scale bar: 100 µm.

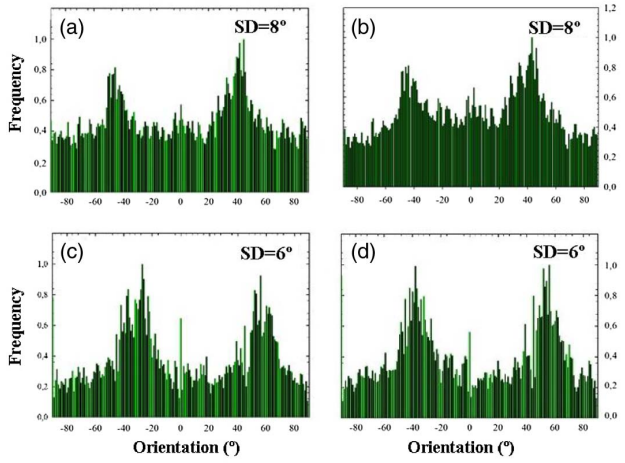

Fig. 6. Histograms of preferential orientation computed from the images in Fig. 5. Left and right plots correspond to the SHG images recorded with lasers #1 and #2, respectively. The SD values are also included for direct comparisons.

collagen fibers. The histograms show two preferential orientations (see the peaks) that do not differ between the images acquired with the two illumination devices. Moreover, the SD values are also similar and indicate that the samples present a high degree of organization (SD < 20°) [18]. This corroborates the successful performance of the laser #2 (fiber-based) when compared to that of the laser #1 (solid state).

B. Adaptive Optics Imaging at Deeper Planes

Due to specimen-induced aberrations, the effectiveness of MP microscopy is reduced when imaging planes located at deeper locations [17,23]. This decrease in image quality with depth can be seen in Fig. 7 for TPEF images of a piece of cellulose recorded with both laser sources. For this part of the experiment the mirrors FM2 and FM3 (see Fig. 1) are introduced in the incoming pathway and the light beam travels across the AO module.

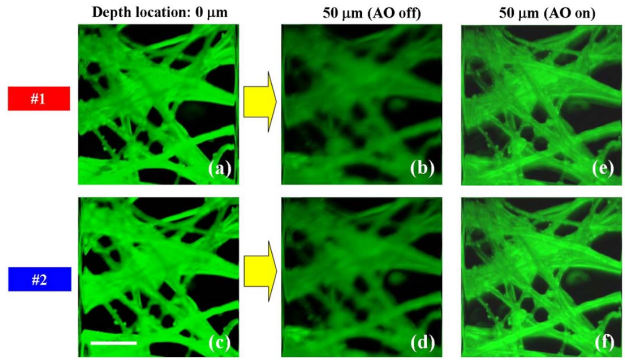

Fig. 7. TPEF images acquired with lasers #1 (upper panels) and #2 (bottom panels) at (a), (c) 0 and (b), (d) 50 µm without the AO module in operation. (e), (f) At 50-µm depth the images were improved by correcting for spherical aberration. Scale bar: 100 µm. The sample was a stained piece of cellulose. Average laser power used: 4 mW.

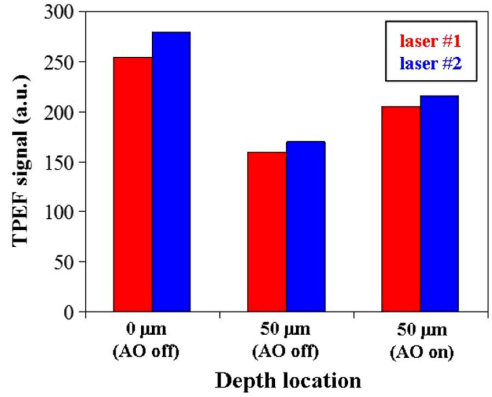

Fig. 8. TPEF intensity corresponding to the images in Fig. 7. See text for more details.

For a shallow plane [Figs. 7(a) and 7(c), 0-µm depth], TPEF images are not affected by aberrations and the total intensity values hardly differ (Fig. 8). However, as expected, at 50-µm depth the TPEF signal is noticeably affected (as shown in Fig. 8). This effect can be over-passed by compensating the aberrations using an AO hill-climbing algorithm [17]. Since spherical aberration has been reported to be the dominant term [17,23–26], this is the unique aberration term that has been corrected during the actual AO operation. After the spherical aberration AO correction (optimum value: –0.5 µm), the quality of the images was greatly increased [Figs. 7(e) and 7(f)]. Moreover, the images registered with the two laser sources were also close to each other. Figure 8 plots a numerical comparison of the total TPEF signal across the images for the different experimental conditions.

4. DISCUSSION AND CONCLUSIONS

In the present work the performance of a 780-nm fs fiber-based laser for MP microscopy has been evaluated and compared to that of a "classical" Ti:sapphire system. Although MP

applications with these types of lasers have been reported in the past, those experiments always used wavelengths longer than 1000 nm [9–15].

Here we have successfully demonstrated that this kind of laser source is appropriate for MP imaging. It has been tested in a variety of biological specimens, including both TPEF and SHG signals. Results show that both laser systems provide similar MP images with quasi-identical structural information. This corroborates that fs fiber-based laser devices are suitable for this imaging microscopy technique.

The utility of this modality of fs lasers when combined with an AO procedure to improve MP images was also tested. In particular, the laser beam aberrations were similar to those of the Ti:sapphire one. Moreover, MP images at different depth locations (with lower quality) also looked alike when comparing both illumination sources. Through the AO operation the spherical aberration was corrected at deeper planes within the sample. After this AO correction, the improved MP images were comparable.

Nowadays, although the probes are becoming smaller, the sources that they use are still bulky, not portable, and require precise alignment. Moreover, they are expensive and the use of chillers for cooling operations is required. These disadvantages can be over-passed by using fs fiber sources with similar technical details as the one analyzed here. However, classical fs lasers also present some advantages, including higher average power (often twice) and tunability. These allow increasing the usefulness of these laser sources mainly in MP applications dealing with opaque or low-transparent samples, where both higher power levels and longer wavelengths [27] are often required. In addition, some recent Ti:sapphire laser models also include an internal pulse compression setup. Pulse shortening operation has been shown to noticeably increase MP imaging performance [28,29].

In conclusion, we have implemented a cost-effective and small fs fiber-based laser system into a MP imaging microscope. This turn-key light source produces a highly stable output and is controlled via a user-friendly interface. Our results show that this device represents an excellent alternative to the broadly used Ti:sapphire lasers and can be used as an efficient tool in different MP microscopy applications. The combination of these compact lasers with MP imaging prototypes of reduced dimensions [30] will allow the potential development of clinical instruments oriented to *in vivo* application in fields such as ophthalmology and neurobiology.

Funding. Secretaría de Estado de Investigación, Desarrollo e Innovación (SEIDI) (FIS2016-76163-R); H2020 European Research Council (ERC) (ERC-2013-AdG-339228); Fundación Séneca (f SéNeCa) (19897/GERM/15).

Acknowledgment. The authors greatly appreciate the help of Mathias Handloser and Jan Schäfer from TOPTICA Photonics.

REFERENCES

1. W. Denk, J. H. Strickler, and W. W. Webb, "Two-photon laser scanning fluorescence microscopy," Science **248**, 73–76 (1990).
2. F. Helmchen and W. Denk, "Deep tissue two-photon microscopy," Nat. Methods **2**, 932–940 (2005).
3. Y. Guo, P. P. Ho, H. Savage, D. Harris, P. Sacks, S. Schantz, F. Liu, N. Zhadin, and R. R. Alfano, "Second-harmonic tomography of tissues," Opt. Lett. **22**, 1323–1325 (1997).
4. P. J. Campagnola, H. A. Clark, W. A. Mohler, A. Lewis, and L. M. Loew, "Second-harmonic imaging microscopy of living cells," J. Biomed. Opt. **6**, 277–286 (2011).
5. M. Göppert-Mayer, "Über Elementarakete mit Zwei Quantensprüngen," Ann. Phys. **401**, 273–294 (1931).
6. M. Oheim, D. J. Michael, M. Geisbauer, D. Madsen, and R. H. Chow, "Principles of two-photon excitation fluorescence microscopy and other nonlinear imaging approaches," Adv. Drug Deliv. Rev. **58**, 788–808 (2006).
7. G. Hall, K. B. Tilbury, K. R. Campbell, K. W. Eliceiri, and P. J. Campagnola, "Experimental and simulation study of the wavelength dependent second harmonic generation of collagen in scattering tissues," Opt. Lett. **39**, 1897–1900 (2014).
8. M. E. Fermann and I. Hartl, "Ultrafast fibre lasers," Nat. Photonics **7**, 868–874 (2013).
9. A. C. Millard, P. W. Wiseman, D. N. Fittinghoff, K. R. Wilson, J. A. Squier, and M. Muller, "Third-harmonic generation microscopy by use of a compact, femtosecond fiber laser source," Appl. Opt. **38**, 7393–7397 (1999).
10. J. R. Unruh, E. S. Price, R. G. Molla, R. Q. Hui, and C. K. Johnson, "Evaluation of a femtosecond fiber laser for two-photon fluorescence correlation spectroscopy," Microsc. Res. Tech. **69**, 891–893 (2006).
11. S. Tang, J. Liu, T. B. Krasieva, Z. Chen, and B. J. Tromberg, "Developing compact multiphoton systems using femtosecond fiber lasers," J. Biomed. Opt. **14**, 030508 (2009).
12. G. J. Liu, K. Kieu, F. W. Wise, and Z. P. Chen, "Multiphoton microscopy system with a compact fiber-based femtosecond-pulse laser and handheld probe," J. Biophoton. **4**, 34–39 (2011).
13. B. Nie, I. Saytashev, A. Chong, H. Liu, S. Arkhipov, F. Wise, and M. Dantus, "Multimodal microscopy with sub-30 fs Yb fiber laser oscillator," Biomed. Opt. Express **3**, 1750–1756 (2012).
14. E. Perillo, J. McCracken, D. Fernée, J. Goldak, F. Medina, D. Miller, H. Yeh, and A. Dunn, "Deep in vivo two-photon microscopy with a low cost custom built mode-locked 1060 nm fiber laser," Biomed. Opt. Express **7**, 324–334 (2016).
15. C. Kong, C. Pilger, H. Hachmeister, X. Wei, T. Cheung, C. Lai, T. Huser, K. Tsia, and K. Wong, "Compact fs ytterbium fiber laser at 1010 nm for biomedical applications," Biomed. Opt. Express **8**, 4921–4932 (2017).
16. W. R. Zipfel, R. M. Williams, and W. W. Webb, "Nonlinear magic: multiphoton microscopy in the biosciences," Nat. Biotechnol. **21**, 1369–1377 (2003).
17. M. Skorsetz, P. Artal, and J. M. Bueno, "Performance evaluation of a sensorless adaptive optics multiphoton microscope," J. Microsc. **261**, 249–258 (2016).
18. F. J. Ávila and J. M. Bueno, "Analysis and quantification of collagen organization with the structure tensor in second harmonic microscopy images of ocular tissues," Appl. Opt. **54**, 9848–9854 (2015).
19. J. M. Bueno, B. Vohnsen, L. Roso, and P. Artal, "Temporal wavefront stability of an ultrafast high-power laser beam," Appl. Opt. **48**, 770–777 (2009).
20. J. M. Bueno, E. J. Gualda, and P. Artal, "Adaptive optics multiphoton microscopy to study ex vivo ocular tissues," J. Biomed. Opt. **15**, 066004 (2010).
21. J. M. Bueno, M. Skorsetz, S. Bonora, and P. Artal, "Wavefront correction in two-photon microscopy with a multi-actuator adaptive lens," Opt. Express **26**, 14278–14287 (2018).
22. J. M. Bueno, E. J. Gualda, and P. Artal, "Analysis of corneal stroma organization with wavefront optimized nonlinear microscopy," Cornea **30**, 692–701 (2011).
23. D. Débarre, E. J. Botcherby, T. Watanabe, S. Srinivas, M. J. Booth, and T. Wilson, "Image-based adaptive optics for two-photon microscopy," Opt. Lett. **34**, 2495–2497 (2009).
24. M. A. A. Neil, R. Juskaitis, M. J. Booth, T. Wilson, T. Tanaka, S. Kawata, and R. Juškaitis, "Adaptive aberration correction in a two-photon microscope," J. Microsc. **200**, 105–108 (2000).

25. L. Sherman, J. Y. Ye, O. Albert, and T. B. Norris, "Adaptive correction of depth-induced aberrations in multiphoton scanning microscopy using a deformable mirror," J. Microsc. **206**, 65–71 (2002).
26. J. M. Bueno, M. Skorsetz, R. Palacios, E. J. Gualda, and P. Artal, "Multiphoton imaging microscopy at deeper layers with adaptive optics control of spherical aberration," J. Biomed. Opt. **19**, 11007 (2014).
27. J. M. Bueno, F. J. Ávila, and P. Artal, "Comparison of second harmonic microscopy images of collagen-based ocular tissues with 800 and 1045 nm," Biomed. Opt. Express **8**, 5065–5074 (2017).
28. P. Xi, Y. Andegeko, D. Pestov, V. V. Lovozoy, and M. Dantus, "Two-photon imaging using adaptive phase compensated ultrashort laser pulses," J. Biomed. Opt. **14**, 14002 (2009).
29. M. Skorsetz, P. Artal, and J. M. Bueno, "Improved multiphoton imaging in biological samples by using variable pulse compression and wavefront assessment," Opt. Commun. **422**, 44–51 (2018).
30. P. Artal, F. J. Ávila, and J. M. Bueno, "Second harmonic generation microscopy of the living human cornea," Proc. SPIE **10498**, 1049810 (2018).

155.54.13.9 {ts '2019-05-07 02:58:25'}